IEEE Access
Multidisciplinary ⋮ Rapid Review ⋮ Open Access Journal

Received November 8, 2019, accepted December 30, 2019, date of publication January 9, 2020, date of current version January 17, 2020.

Digital Object Identifier 10.1109/ACCESS.2020.2965197

Analysis of Discharge Faults Between Flanges Caused by Transient Enclosure Voltage

JISHENG LI[1], ZEYU HE[2], YU WANG[2], XIAOYUE CHEN[2], AND YONGCONG LIU[2]

[1]Daya Bay Nuclear Power Operations and Management Company, Ltd., Shenzhen 518124, China
[2]School of Electrical and Automation, Wuhan University, Wuhan 430072, China

Corresponding author: Yu Wang (yuwang@whu.edu.cn)

ABSTRACT An increase in transient enclosure voltage can threaten the personal safety of workers and the normal operation of secondary equipment and may cause discharge between the flanges of gas insulated switchgear (GIS) enclosures. This study considered the spark–discharge fault between GIS enclosure flanges of a 500-kV nuclear power plant in China when the disconnect switch is operated in the background. The dynamic arc model during the operation of the disconnect switch was improved in this study, and the equivalent calculation model of transient enclosure voltage (TEV) caused by very fast transient overvoltage generated during the operation of the disconnect switch was established using the electromagnetic transient program ATP-EMTP. Suppression measures of the discharge phenomena were also discussed. The results demonstrated that the transient enclosure voltage caused by the operation of the disconnect switch can reach 75 kV in the most severe case, which causes discharge between the flanges. Reducing the residual charge on the island side of the disconnect switch, installing a metal oxide arrester, and reducing the inductance of the ground wire have different inhibitory effects on this discharge phenomenon, but they all have their limitations. The most simple and effective control measure is to use a short joint between two flanges. The study conclusions can be used as reference for preventing such discharge phenomena.

INDEX TERMS Transient enclosure voltage, discharge between flanges, improved arc model, inhibition of measures.

I. INTRODUCTION

Gas insulated switchgear (GIS) is used increasingly at all voltage levels because of its safety, reliability, small floor area, and less work on overhaul. However, the operation of the disconnect switch in GIS generates very fast transient overvoltage (VFTO), with high frequency, amplitude, and gradient, which can threaten the insulation safety of the GIS body and adjacent high-voltage equipment (such as transformers). In addition, the transmission of VFTO causes transient enclosure voltage (TEV). As voltage level improves, insulation problems caused by TEV become more severe and can cause personal injury to workers. Moreover, electromagnetic radiation generated by TEV can interfere with secondary equipment, causing misoperation or even failure. The suppression of TEV has attracted an increasing amount of attention.

According to statistics from the International Council on Large Electric Systems (CIGRE), more than half of the substations in the world have experienced transient ground potential increase [1]. During the commissioning process of a 1000-kV Hybrid GIS (HGIS) at the China Nanyang UHV substation, a discharge phenomenon at the grounding switch gate caused by TEV occurred [2]. The 1000-kV GIS test platform at the UHV AC test base of Wuhan State Grid of China also experienced an accident in which a high TEV damaged the gas density sensor on the GIS enclosure [2]. In March 2017, an accident occurred in a 500-kV GIS nuclear power plant in China, causing spark discharge between the flanges of the outlet casing of the contact transformer because of the operation of the disconnect switch, as shown in Fig. 1. According to the preliminary analysis of the field situation, the length of the grounding wire of the two flanges above and below the discharge point is different. The discharge may have occurred because of the TEV generated on the GIS housing during the operation of the disconnect switch. When TEV is transmitted to the flange, a large potential difference is formed between the flanges, which results in discharge because the impedance of the ground wire cannot be ignored at high frequencies.

The associate editor coordinating the review of this manuscript and approving it for publication was Ravindra Singh.

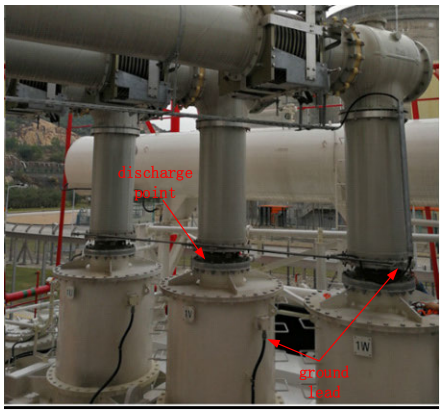

FIGURE 1. GIS enclosure discharge structure diagram.

Numerous studies have researched the operation of the disconnect switch to produce TEV. Ford and Geddes [3] calculated the mechanism of TEV increase in GIS based on the multiconductor transmission line theory and studied the influence of TEV on adjacent equipment and staff. Based on theoretical analysis and experimental measurement, Fujimoto et al. [4] conducted in-depth research on TEV generation and propagation mechanisms and related characteristics in GIS. Dick et al. [5] further analyzed, calculated, and simulated TEV; deduced transient potential from shell structure; and proposed modifications to operating procedures, changes to the GIS configuration, and other suppression measures. Guan *et al.* [6] studied the relationship between TEV and VFTO through experimental methods. TEV amplitude at different locations on the test circuit was analyzed by introducing the scale coefficient, and the origin of TEV by traveling wave transmission theory was verified. Lin *et al.* [7], [8] combined a GIS shell model with an internal transient model by using phase mode transformation and studied the influence of different operation modes and grounding modes on TEV amplitude. Through calculation, Boggs *et al.* [9]–[12] proposed relevant control factors of TEV; in other words, TEV is inversely proportional to soil resistivity and proportional to residual charge, grounding grid depth, grid number, total grid area, and length of grounding wire. Hu et al. [13]–[15] developed a measuring device for TEV based on the resistance voltage divider and studied the influence of different disconnect switch speeds, residual charges, branch bus lengths, and isolation switch wiring modes on TEV through multiple measurements. Shimoda *et al.* [16], [17] verified the inhibition performance of zinc oxide (ZnO) on TEV through field tests.

The reliability of TEV calculation is mainly affected by the accuracy of VFTO calculation. In studies and calculations of VFTO, simplified models, such as static resistance and time-varying resistance models, are often used for the dynamic process of operating the isolation switch. They have specific accuracies, but the models are simple and cannot accurately describe the process of arc occurrence, resulting in deviation of the results. In addition, previous calculations have mainly studied TEV caused by a single VFTO pulse, and the waveform was relatively single. Few studies have focused on TEV generated by multiple pulse superpositions with different amplitudes and waveforms in actual operation, which leads to a large deviation between the calculated results and the actual situation. Therefore, this paper presents an improved arc model considering the energy conversion process and the influence of arc current in the process of arc generation and combines the VFTO calculation model with the TEV calculation model to obtain TEV generated by multiple pulses of complex waveforms.

Based on the phenomenon of discharge between flanges in a 500-kV nuclear power plant in China, the first section presents an analysis of the generation and calculation principle of TEV. In Section 2, the dynamic model of the disconnect switch is improved after considering the energy conversion process and the influence of the arc current in the process of arc generation, and the corresponding GIS internal VFTO and shell TEV equivalent calculation models are constructed by ATP-EMTP software. To obtain the actual TEV waveform, the third section combines the VFTO calculation model with the TEV calculation model. The effect of TEV on discharge between flanges caused by refraction and reflection of actual VFTO waveform propagation to the transformer bushing is studied. The fourth section analyzes and compares the inhibition effects of different discharge inhibition measures and obtains the most effective ones. The calculation results in this paper have great reference value for preventing this type of phenomenon.

II. CALCULATION PRINCIPLE OF TEV

Disconnect switch operation in GIS produces VFTO with a steep front on both sides and a rise time of approximately 4–10 ns. Due to the strong skin effect, it is transmitted along the primary bus and the inner surface of the GIS shell. When the high-frequency transient wave propagates to the shell discontinuity, it is reflected to the outer wall of the shell through refraction and reflection, causing TEV. Typical discontinuities are the connection between the GIS and main transformer casing as well as the connection between the overhead line and outgoing casing.

Although the GIS shell is grounded during operation, due to the high-frequency characteristics of TEV, the grounding lead and ground grid cannot be considered in terms of centralized parameters during the high-frequency transient process; thus, the shell cannot be effectively kept at zero potential. The transient shell potential contains a variety of frequency components and a high amplitude, which, if unchecked, will cause discharge between the housing and the ground wire and the insulation flange.

When GIS is connected to sulfur hexafluoride (SF_6) or casing of the transformer, because the GIS and transformer typically belong to two different manufacturers, the shell is discontinuous. The conventional method is to connect GIS three-phase shells with copper bars, and transformer three-phase shells are also connected and grounded. In this system, although the power frequency induced current flowing

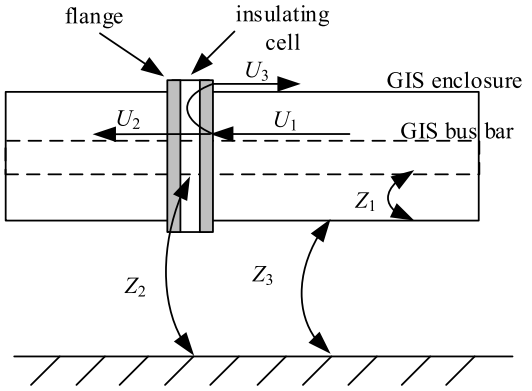

FIGURE 2. Simplified model of wave process.

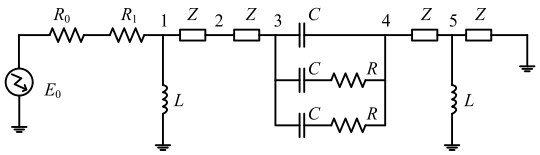

FIGURE 3. TEV calculation circuit model.

through the GIS shell is zero, VFTO is refracted and reflected here, which can easily cause TEV. Spark discharge occurs between GIS and transformer flanges during the operation of individual disconnect switches. The simplified wave process at this point is shown in Fig. 2. Part of the transient electromagnetic process occurs in the internal circuit and is composed of the wave impedance between the high-voltage bus and the inner wall of the shell and the equivalent model of each electrical element. The equivalent wave impedance of this circuit is Z_1. The other part occurs in the external circuit and is composed of the wave impedance between the transformer casing and the earth Z_2 and that between the outer wall of the shell and the earth Z_3. Peterson's Law can be used to roughly calculate the voltage refracted to the GIS shell:

$$U_3 = -2U_0 \frac{Z_3}{Z_1 + Z_2 + Z_3} \tag{1}$$

The equivalent circuit for simulation calculation was obtained according to the transmission line model proposed by Dick *et al.*, as shown in Fig. 3. In the figure, power supply E_0 and R_1 are used to simulate the case when a VFTO of 1.0 p.u. produced by GIS isolation switch operation reaches the casing. R_2 is the wave impedance between the transformer casing and the earth. The grounding wires on both sides of the flange are equivalent to inductance L. Capacitance C and resistance R at junctions 3 and 4 are high-frequency transient models of insulation flange.

However, this model can only simulate the TEV generated under a single pulse of VFTO, and the amplitude and waveform deviate from the actual situation. To calculate the actual TEV more accurately, this study combined the VFTO generating circuit with the TEV calculating circuit and added the VFTO generated by operating the disconnect switch directly to the equivalent model of the GIS shell. In other words, this study replaced the E and R_1 in Fig. 3.

III. TEV CALCULATION MODEL BUILDING

The VFTO produced by the GIS disconnect switch has a high frequency and wide range. Only in the frequency range of VFTO occurrence can simulation be performed for each component of the system to ensure the accuracy of calculation. In addition, the complex structure and large volume of GIS equipment make avoiding errors in component model establishment and equipment parameter selection difficult. Therefore, the accumulated errors will make the final calculation results have a large deviation. Such data are meaningless to the development, manufacture, and operation of GIS equipment. Therefore, the equivalence of the equipment in the model is crucial.

A. MODELING OF EACH COMPONENT

The key point in the calculation of TEV is to establish the equivalent model of each component in GIS. The equivalent models of each component adopted in this paper is as follows.

1) MODEL OF BUSBAR

GIS bus can be simulated using a nondestructive uniform transmission line model. The calculation formula of the wave impedance of the coaxial busbar conductor shell or cable conductor and shielding body in a GIS substation is expressed in (2):

$$Z_1 = 60 \ln \frac{R_1}{R_2} \tag{2}$$

where R_1 is the inner radius of the GIS shell, and R_2 is the radius of the inner conductor. The calculation formula of the impedance of the shell-to-ground wave is shown in (3):

$$Z_2 = 60 \ln \frac{2h}{R_3} \tag{3}$$

where R_3 is the outer radius of GIS shell, and h is the height of GIS shell.

2) MODEL OF DISCONNECTING SWITCH ARC

The accuracy of the calculation is affected by the accurate simulation of arc occurrence. The traditional arc model takes few factors into consideration; although it is simple and easy to use, it is somewhat deficient in computational accuracy. Therefore, this study improved the traditional segmented arc model based on the Cassie–Mayr arc model. The influence of arc heat dissipation power and arc current were considered in the description of arc channel resistance. This arc model can effectively simulate the whole process of arc burning and improve calculation accuracy.

For the pre-breakdown stage of the improved dynamic arc model, considering the breakdown delay t_δ, a hyperbolic arc resistance expression is adopted as follows:

$$R_a = r_0 + 2Z(\frac{t_\delta}{t} - 1), \quad 0 < t < t_\delta \tag{4}$$

where R_0 is the arc static resistance, generally between 0.5 Ω and 2 Ω, Z is the GIS busbar wave impedance, and t_δ is the

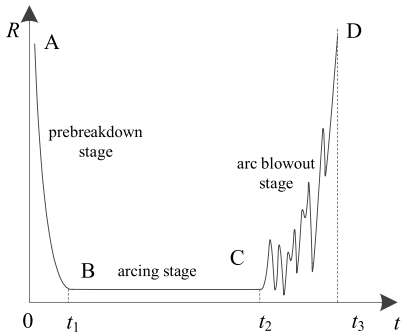

FIGURE 4. Improved resistance variation curve of dynamic arc model.

breakdown time for the fracture. According to equation (4), the arc channel resistance before breakdown is infinite, and the resistance drops to static resistance r_0 after breakdown.

In the arc-quenching stage, combined with the Cassie–Mayr arc model, the description function of the dynamic process of arc quenching can be expressed as:

$$\frac{dg}{dt} = \frac{1}{\tau(g)}\left(\frac{i^2}{P(g)} - g\right) \tag{5}$$

where g is the arc conductance, i is the arc current, $P(g)$ is the arc heat dissipation power, and τ(g) is the arc time constant. Among them, heat dissipation power $P(g)$ and the time constant $\tau(g)$ play decisive roles in arc quenching. They are both functions of arc conductance, whose values are related to temperature, type and design of circuit breaker, and other factors, and they are defined as the following power functions of conductance:

$$\begin{aligned} \tau(g) &= \tau_0 g^{\alpha} \\ P(g) &= P_0 g^{\beta} \end{aligned} \tag{6}$$

where the types of τ_0, P_0, α, and β are constant.

The arc heat dissipation power $P(g)$ and time constant $\tau(g)$ can be calculated as constants at very small time intervals. The first-order differential equation can be obtained through Euler's method as follows:

$$g(t + \Delta t) = g(t) + \left(\frac{i^2}{P(g)} - g(t)\right)\left[1 - e^{-\frac{\Delta t}{\tau(g)}}\right] \tag{7}$$

MODELS modules and languages included in ATP-EMTP software were used. The dynamic arc theory basis was substituted into the improved Euler's method formula to perform the programming. The control function according to the dynamic arc model was realized and the arc reignition model of the isolation switch was obtained. The characteristic curve derived from the theory is as follows:

Compared with the traditional piecewise resistance model, the characteristic curve of this model is different mainly in that the rise of arc channel resistance is oscillatory in the arc-quenching stage. This is because the model is based on the Cassie–Mayr arc model, which accounts for the process of energy conversion and the influence of arc current during arc quenching. However, these factors, especially the current, tend to be unstable, which causes the arc resistance to increase in an oscillating manner.

3) MODEL OF CIRCUIT BREAKER

The closed circuit breaker is considered part of the transmission line as the disconnect switch. The capacitance between the breaks and the capacitance to the ground is used to simulate the disconnection.

4) MODEL OF TRANSFORMER

The results of the equivalent transformer with inlet capacitance in the calculation model agree well with those of other complex models; thus, the transformer is equivalent to the ideal power supply, the inlet capacitance, and the equivalent inductance.

The inlet equivalent capacitance Ci of a transformer is related to its voltage grade, capacity, and structure. In general, the higher the voltage level and the higher the rated power of the transformer, the higher the equivalent capacitance of the inlet. The empirical formula is expressed as follows (8):

$$C_i = K\sqrt[n]{S} \tag{8}$$

where the unit of capacitance is pF and S is the three-phase capacity (MVA) of the transformer. $n = 4$ in the voltage rating system above 500 kV; $n = 3$ in the voltage rating system with 220 kV rating and below; $K = 800$ in the 750 kV voltage rating system; $K = 940$ in the 500 kV voltage rating system.

5) MODELS OF OTHER COMPONENTS

Insulators, voltage transformers, lightning arresters, and other components can be represented by ground capacitance with concentrated parameters, and bushing can be represented by transmission line and ground capacitance.

Because the whole system is approximately three-phase symmetric, a single-phase circuit can be used for simulation. According to the data provided by the cooperative units, the GIS power station equipment parameters and equivalent models studied in this paper are shown in Tables 1 and Tables 2, respectively.

TABLE 1. Equivalent parameters of equipment in the substation.

Equipment	Code	Equivalent parameters
Transformer	TR3	Earth capacitance 1500pF
Circuit breaker	CB	Fracture capacitance 520 pF/ Earth capacitance 28.5pF
Disconnect switch	DS	Fracture capacitance 20pF
Potential transformer	PT	50pF
Surge arrester	MOA	43 pF(PSA444F)
Earth switch	ES	45pF

B. VERIFICATION OF MODEL CORRECTNESS

In order to verify the accuracy of the calculation model, this section compares and analyzes the simulation results of this paper with the measured data of the literature tests.

Chen *et al.* [18] established a VFTO test loop for UHV GIS equipment that could generate relatively severe VFTO, and they make a lot of experimental

TABLE 2. Equivalent model of equipment in substation.

Equipment	Code
GIS bus	
Disconnect switch	
Circuit breaker	
Transformer	
Potential transformer	

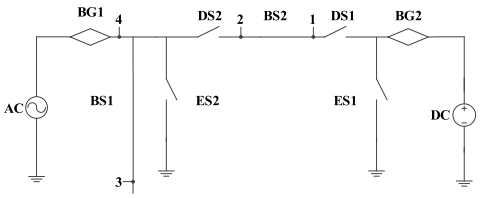

FIGURE 5. Schematic diagram of test platform circuit.

TABLE 3. Simulation results.

Measurement point	Measured value (p.u.)	Simulation value (p.u.)
1	0.28	0.23
2	0.23	0.18
3	0.19	0.15
4	0.14	0.11

measurements on the VFTO. The circuit schematic diagram is shown in Fig. 5:

According to the modeling method mentioned above, an equivalent model of the test platform was built in ATP-EMTP. Since the GIS equipment parameters were not given in the literature [18], the selection was carried out according to the empirical parameters, and the improved dynamic arc model built in this paper is used in the process of generating arc by operating disconnecting switch. The calculated results are shown in Table 3:

By comparing the calculated results with the measured results, it can be found that the maximum VFTO amplitude obtained by simulation is larger than that obtained by experiment. This is because in the process of simulation calculation, due to the high frequency characteristic of VFTO, the influence of its resistance is ignored in the modeling of each equipment. In addition, since the equipment parameters were not provided in the literature, all parameters used in the simulation calculation were selected according to the empirical value, which would bring certain result errors. Typical single-breakdown waveforms obtained by experiment and simulation are shown in Fig. 6 and Fig. 7.

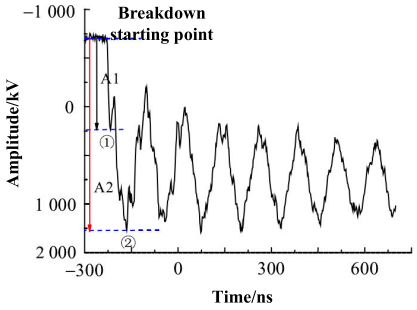

FIGURE 6. Typical waveforms of single breakdown obtained by experiment.

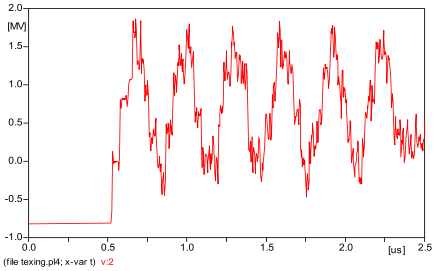

FIGURE 7. Typical waveforms of single breakdown obtained by simulation.

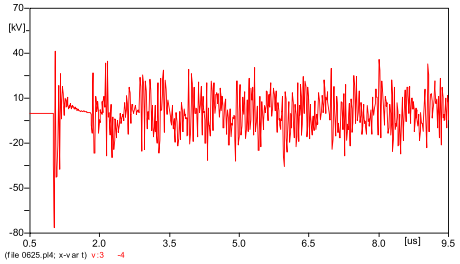

FIGURE 8. TEV at the interface of GIS and transformer.

By comparing Fig. 6 and Fig. 7, it can be seen that the overall change and oscillation trend of the waveform obtained by simulation are very close to the waveform measured by experiment. Their oscillation frequency is basically the same, the main frequency is about 5MHz, and the oscillation amplitude will gradually decrease as time goes by, which proves the accuracy of the arc model and the equivalent calculation model of other equipment.

IV. CALCULATION RESULT OF TEV

In the calculation, the overvoltage generated by switching is considered in the most severe case, that is, the switch is closed when the residual charge of −1.0 p.u. is on the island side of the disconnect switch, and the voltage of the power station side of the isolation switch is +1.0 p.u. At this time, the VFTO overvoltage level generated is the highest, which theoretically can reach 3.0 p.u., and the TEV generated by it is also the most severe. Fig. 8 shows the TEV of the flange at the GIS–transformer interface in this case.

According to these results, the maximum voltage between the flanges reached 75 kV when the disconnect switch

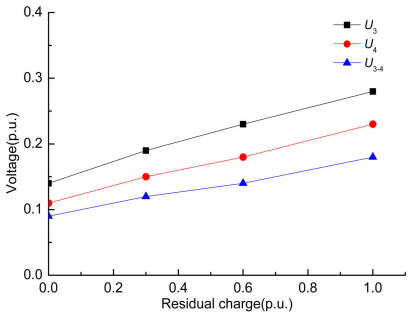

FIGURE 9. Relation of TEV to residual charge.

TABLE 4. Influence of residual charge on TEV.

Residual charge(p.u.)	U_3(p.u.)	U_4(p.u.)	$U_{3\text{-}4}$(p.u.)
1.0	0.28	0.23	0.18
0.6	0.23	0.18	0.14
0.3	0.19	0.15	0.12
0	0.14	0.11	0.09

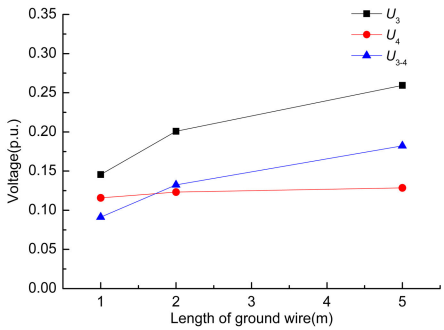

FIGURE 10. Relationship between TEV and grounding wire length.

TABLE 5. Effect of grounding wire length on TEV.

Length(m)	U_3(p.u.)	U_4(p.u.)	$U_{3\text{-}4}$(p.u.)
5	0.25	0.12	0.18
2	0.20	0.12	0.13
1	0.14	0.11	0.09

was operated in the most severe case, exceeding the surface flashover voltage (∼20 kV) of the insulation partition between the flanges of the power station, which causes discharge between the flanges.

V. ANALYSIS OF FACTORS INFLUENCING TEV

On the basis of the above calculation model, the TEV of different residual charge and grounding wire length was calculated by changing the component parameters in the model. The influence of residual charge and length of grounding wire on TEV was analyzed through calculation results, and the corresponding influence law was obtained.

A. EFFECT OF RESIDUAL CHARGE ON TEV

In practical operation, the residual charge on the island side of the isolation switch is easily discharged through electromagnetic voltage transformers and other devices; thus, the voltage in the island is often less than 1.0 p.u. at the moment of closing. Table 4 and Fig. 9 shows the amplitude of TEV under different residual charges.

The results demonstrate that reducing the residual charge on the island side can effectively reduce the TEV amplitude. Therefore, before operation of the disconnect switch, the residual charge can be discharged using the grounding switch to reduce the amplitude of TEV.

According to the data provided by the cooperative unit, the residual voltage on the island side before the disconnect switch closes is approximately 10 kV. In this case, a voltage of 1.0 p.u. is still selected from the side of the power station after careful consideration, and the maximum voltage between the flanges is calculated to be approximately 40 kV, which still causes discharge between the flanges.

B. EFFECT OF GROUNDING WIRE LENGTH ON TEV

Due to the high frequency of TEV, the inductance effect of grounding wire cannot be ignored. The TEV is reflected and refracted at the ground point, but because the wave impedance of the ground wire is in parallel with the ground wave impedance of the GIS enclosure, which reduces the ground wave impedance of this point, the refracted wave voltage can be reduced. Table 5 and Fig. 10 presents the influence of changing the inductance of grounding wire at node 2 on TEV.

The results reveal that reducing the inductance of the ground wire can effectively suppress TEV, and the closer the position to the ground wire is, the more obvious the suppression effect is. In practical application, GIS enclosure grounding wires can be installed at locations with severe TEV to suppress the TEV of the GIS as a whole. However, even if the inductance of the ground wire is reduced, for example, by 1 μH, then the maximum voltage difference between the flanges would be approximately 38 kV and discharge may occur.

VI. SUPPRESSION MEASURES FOR THE DISCHARGE PHENOMENON

The power station studied here prepared two insulation intervals, which were located in the GIS side flange and transformer side riser flange (discharge point), respectively. Because piezoresistors were connected in parallel on both sides of the GIS side flange, the inhibition effect of installing metal oxide arresters (MOAs) and short connections on both sides of the flange on the transformer side to the discharge phenomenon is calculated.

A. INSTALL MOA BETWEEN FLANGES

1) MODEL DESCRIPTION

MOAs have a steep wave response, which can be used to suppress VFTO on bus and TEV caused by VFTO. To solve the discharge problem, MOAs are added between the flanges to suppress TEV between them. The transient calculation model is shown in Fig. 11.

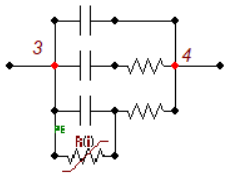

FIGURE 11. Transient model of MOA installed between flanges.

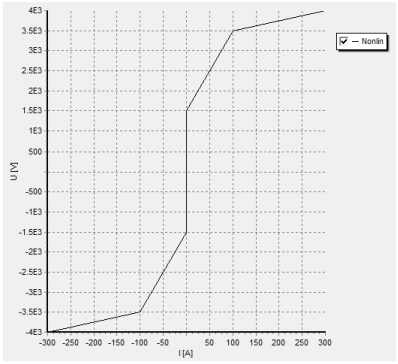

FIGURE 12. Volt-second characteristics of MOAs.

TABLE 6. Effect of bonded MOA on TEV.

Operating voltage (kV)	U_3(kV)	U_4(kV)	$U_{3\text{-}4}$(kV)
10	54.2	37.7	16.5
5	50.5	41.3	9.3
1.5	48.1	44.1	4.0

2) PARAMETER SETTINGS

The high frequency transient model of insulation flange between junction 3 and junction 4 in Fig. 11 is equivalent by capacitance(20pF) and resistance(1Ω) [16]. A nonlinear resistance is used to simulate MOAs in parallel between flanges, and its volt-second characteristics are shown in Fig. 12.

3) CALCULATION RESULTS

The suppression effect of MOAs with different operating voltages across flanges on TEV is shown in Table 6.

According to the results, adding MOAs between flanges can effectively suppress the potential difference caused by TEV between them, and the lower the operating voltage, the greater the suppression effect. However, in practical application, the reference voltage of MOA should be properly selected to avoid overheating damage of MOA under power frequency fault current. In addition, due to the small discharge voltage, cooperating within the parameters of MOA is difficult. If the parameters do not match, it may lead to frequent MOA action or refusal to action.

B. ADD SHORT JOINTS BETWEEN FLANGES

The discharge phenomenon of the GIS power station studied here is caused by the potential difference between flanges of TEV. To eliminate this potential difference, the method of short splicing between flanges was considered. The added short joints and the original three-phase splice may cause

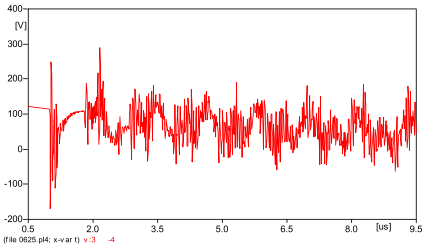

FIGURE 13. Voltage between flanges after adding short joints.

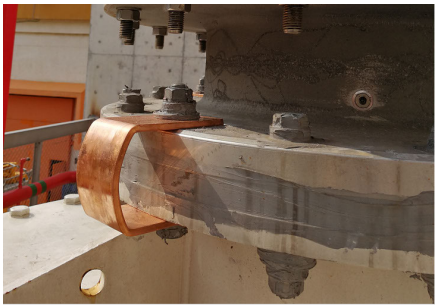

FIGURE 14. Flange layout after bonding.

circulation between the shells, thus canceling the three-phase splice. The calculation results after short connection are shown in Fig. 13.

The results demonstrate that the straddling copper bar can significantly reduce the voltage between flanges, but cannot reduce the TEV between the flanges and the ground. Because the discharge phenomenon studied here occurs between flanges and the TEV on the ground does not cause discharge, this method is the most effective for the power station studied. The flange of the elevated seat of the transformer after bonding is shown in Fig. 14. After bonding, no discharge is caused under the same operation mode, which proves that this solution is effective.

VII. CONCLUSION

This study investigated the phenomenon of spark discharge between flanges caused by operation of an isolation switch in a 500-kV nuclear power plant in China. The TEV caused by operating the isolation switch and its inhibition measures were studied, and the following conclusions were obtained:

(1) Based on the Cassie–Mayr arc model, this study improved the traditional piecewise arc model. Operating the disconnect switch in the most severe case can generate a potential difference of 75kV between GIS housing flanges, which causes spark discharge.

(2) Reducing the residual charge on the island side of the isolation switch and reducing the inductance of the ground wire can reduce the TEV amplitude to different degrees. However, these measures have their own limitations; they cannot significantly suppress the voltage between the flanges, but they may still cause discharge between the flanges.

(3) To suppress discharge between flanges caused by TEV, using short joints for bonding is the simplest and most

effective method. This method can effectively suppress the voltage difference between flanges and prevent the discharge phenomenon. However, checking the type selection of the short connector and canceling the original three-phase short connector is necessary to avoid circulation.

REFERENCES

[1] Z. Zhang, G. Liang, X. Cui, and M. Wu, "The effects of operations of the disconnector switch on the secondary circuits in gas insulated substations," *High Volt. Eng.*, vol. 28, no. 2, pp. 154–196, Feb. 2002.
[2] R. Hu, "Research on the characteristics of electromagnetic transient generated during switching of disconnector in AC ultra high voltage gas insulated switchgear," Ph.D. dissertation, School Elect. Electron. Eng., North China Electr. Power Univ., Beijing, China, 2016.
[3] G. Ford and L. Geddes, "Transient ground potential rise in gas insulated substations–assessment of shock hazard," *IEEE Trans. Power App. Syst.*, vols. PAS–101, no. 10, pp. 3620–3629, Oct. 1982.
[4] N. Fujimoto, E. Dick, S. Boggs, and G. Ford, "Transient ground potential rise in gas insulated substations–experimental studies," *IEEE Trans. Power App. Syst.*, vols. PAS–101, no. 10, pp. 3603–3609, Oct. 1982.
[5] E. Dick, N. Fujimoto, G. Ford, and S. Harvey, "Transient ground potential rise in gas-insulated substations–problem identification and mitigation," *IEEE Trans. Power App. Syst.*, vols. PAS–101, no. 10, pp. 3610–3619, Oct. 1982.
[6] Y. Guan, Y. Cai, W. Liu, and W. Chen, "The relationship between VFTO and shell potential increase caused by GIS isolation switch operation," *High Volt. Eng.*, vol. 41, no. 12, pp. 4097–4104, Dec. 2015.
[7] X. Lin, S. Li, J. Xu, and Q. Cai, "Simulation of transient enclosure voltage in EHV GIS," *High Volt. App.*, vol. 47, no. 3, pp. 12–17, Mar. 2011.
[8] J. Xu, L. Wang, and S. Li, "Simulation and analysis of enclosure voltage transient characteristic caused by disconnector operation in ultra high voltage gas insulated switch," *High Volt. Eng.*, vol. 38, no. 2, pp. 288–294, Feb. 2012.
[9] S. A. Boggs, F. Y. Chu, N. Fujimoto, A. Krenicky, A. Plessl, and D. Schlicht, "Disconnect switch induced transients and trapped charge in gas-insulated substations," *IEEE Trans. Power App. Syst.*, vols. PER–2, no. 10, pp. 3593–3602, Oct. 1982.
[10] R. S. Gorayan and K. Chandrakar, "Analysis and control of transient enclosure voltages in GIS (EMTP simulation studies)," in *Proc. Annu. IEEE India Conf. (INDICON)*, Dec. 2013, pp. 1–6.
[11] A. J. Reid, M. D. Judd, and G. Duncan, "Simultaneous measurement of partial discharge using TEV, IEC60270 and UHF techniques," in *Proc. IEEE Int. Symp. Electr. Insul.*, San Juan, PR, USA, Jun. 2012, pp. 439–442.
[12] H. Prasetia, U. Khayam, Suwarno, A. Itose, M. Kozako, and M. Hikita, "Simulation analysis of surface current as TEV signal caused by partial discharge on post insulator in bus duct," in *Proc. IEEE Int. Conf. Dielectrics (ICD)*, Jul. 2016, pp. 480–484.
[13] Y. Cai, Y. Guan, and W. Liu, "Statistical characteristics of transient enclosure voltage in ultra-high-voltage gas-insulated switchgear," *Plasma Sci. Technol.*, vol. 19, no. 6, Jun. 2017, Art. no. 064011.
[14] R. Hu, X. Cui, W. Chen, W. Zhang, Z. Li, and M. Dai, "Development of the measuring device of transient enclosure voltage in ultra high voltage gas insulated switchgear," *Proc. Chin. Soc. Electr. Eng.* vol. 35, no. 23, pp. 6235–6245, Dec. 2015.
[15] R. Hu, X. Cui, W. Zhang, P. Chen, L. Qi, J. Li, W. Chen, Z. Li, and M. Dai, "Transient enclosure voltage (TEV) measurement system of UHV GIS and TEV statistical characterization," in *Proc. Int. Symp. Electromagn. Compat. (EMC)*, Sep. 2012, pp. 1–6.
[16] N. Shimoda, K. Taguchi, and T. Nemoto, "Suppression of very fast transient overvoltages across insulating flange of 1000 kV GIS," in *Proc. Int. Symp. High Voltage Eng.*, Aug. 2000, p. 1.
[17] J. Zhao, J. Zhang, Z. Liu, and Z. Gan, "Measurement of TEV of 1000kV UHV gas insulated switchgear," in *Proc. 7th Asia–Pacific Conf. Environ. Electromagn. (CEEM)*, Nov. 2015, pp. 313–315.
[18] W. Chen, Z. Li, G. Sun, M. Dai, W. Liu, C. Li, L. Wang, H. Wang, G. Chen, T. Yao, S. Wang, J. Lu, J. Wu, X. Zhang, W. Li, and X. Li, "Experimental research on the characteristics of very fast transient overvoltage in ultra high voltage gas insulated switchgear," *Proc. Chin. Soc. Electr. Eng.*, vol. 31, no. 31, pp. 38–47, Nov. 2011.

JISHENG LI received the B.S. degree in electrical engineering and automation from the Harbin Institute of Technology, Harbin, Heilongjiang, in 1997. His research interest includes improvement and application of electrical technology in nuclear power plant.

ZEYU HE received the B.S. degree in electrical engineering and automation from Fuzhou University, Fuzhou, Fujian, in 2018. He is currently pursuing the M.S. degree in electrical engineering with Wuhan University, Hubei, China. His research interest includes over-voltage and protection of power systems.

YU WANG received the B.S. degree in electrical engineering and automation from Wuhan University, Wuhan, Hubei, in 2006, and the Ph.D. degree in high voltage and insulation technology from Wuhan University, in 2012. In 2018, he went to the Department of Electrical Engineering and Computer Science, University of Tennessee, as a Visiting Scholar.

Since 2016, he has been an Associate Professor with the School of Electrical Engineering and Automation, Wuhan University. His research interests include lightning protection and grounding technology of power systems, overvoltage protection, and disaster prevention and reduction of power grid. He has published more than 50 high-level academic papers, including more than 10 SCI retrieval papers, more than 30 EI retrieval papers, and applied for 14 patents in China.

Dr. Wang is a member of the CIGRE.

XIAOYUE CHEN received the B.S. degree in electrical engineering and automation from Wuhan University, Wuhan, Hubei, in 2008, the M.S. degree in high voltage and insulation technology, and the Ph.D. degree from Wuhan University, in 2010 and 2016, respectively.

Her research interest includes power system over-voltage and electromagnetic environment of power systems.

YONGCONG LIU received the B.S. degree in electrical engineering and automation from Wuhan University, Wuhan, Hubei, in 2018, where he is currently pursuing the M.S. degree in electrical engineering. His research interests include electromagnetic compatibility of power systems and electromagnetic field simulation of power equipment.